

Effects of finite temperature on the magnetized equation of state in neutron stars composed of a Bose-Einstein condensate

G. Quintero Angulo^{1,*}, L. C. Suárez González^{2,†}, A. Pérez Martínez^{3,‡} and H. Pérez Rojas^{2,§}

¹*Facultad de Física, Universidad de la Habana, San Lázaro y L, Vedado, 10400 La Habana, Cuba*

²*Instituto de Cibernética, Matemática y Física (ICIMAF), Calle E esq a 15, Vedado, 10400 La Habana, Cuba*

³*Departamento de Física Fundamental, Universidad de Salamanca, Plaza de la Merced s/n, 37008 Salamanca, Spain*



(Received 10 September 2022; revised 3 March 2023; accepted 1 June 2023; published 27 July 2023)

We study the role of temperature and magnetic field on the equation of state and macroscopic properties of Bose-Einstein condensate stars. These compact objects are composed of a condensed gas of interacting neutral vector bosons coupled to a uniform and constant magnetic field. We found that the main consequence of a finite temperature in the magnetized equations of state is to increase the inner pressure of the star. As a consequence, magnetized hot Bose-Einstein condensate stars are larger and heavier than their zero-temperature counterparts. However, the maximum masses obtained by the model remain almost unchanged, and the magnetic deformation of the star increases with the temperature. Besides, increasing the temperature reduces the number of stable stars, an effect that the magnetic field enhances. The implications of our results for the star's evolution, compactness, redshift, and mass quadrupolar moment are also analyzed.

DOI: [10.1103/PhysRevC.108.015806](https://doi.org/10.1103/PhysRevC.108.015806)

I. INTRODUCTION

Historically, boson star models have been less common than the ones of fermions for the description of compact stars, in particular neutron stars. The main reason behind this was the absence of a realistic candidate for the star-forming boson, and the fact that a star composed of an ideal gas of bosons cannot reach the mass of observed neutron stars unless the mass of the boson is several orders less than that of any known particle [1–3]. Nevertheless, the experimental achievement of Bose-Einstein condensation (BEC) of interacting atomic systems at the end of the last century [4], and the reinforcement of the long-lasting supposition that neutron stars (NS) may mainly consist of a superfluid of neutrons given by the theoretical adjustment of the cooling data of Cassiopeia A [5–7], provided a rebirth of the application of bosons stars models to the study of neutron stars. Paired neutrons inside neutron stars are usually considered as weakly bounded Cooper pairs whose size is of the order of the interparticle distance [Bardeen-Copper-Schrieffer (BCS) limit] [8]. However, considering the neutron pairs as tightly bounded and behaving as effective bosons (BEC limit) led, some years ago, to models of Bose-Einstein condensate stars (BECS) [8–12]. It is worth noticing that, given the NS inner conditions, both situations

may be possible [8]. Here, our focus will be on the second one.

A BECS is a compact object composed of a condensed gas of interacting bosons where gravity is mainly balanced by the pressure that comes from the interactions. The equations of state (EoS) of BECS, as well as their mass and size, are governed by the boson mass m and the interaction strength through the scattering length a [9]. In the context of NS, $m = 2m_n$, m_n being the neutron mass, and the scattering length of the bosons is assumed to range from 1 to 15 fm. With those values of m and a , the model at zero temperature and magnetic field gives stars with maximum masses around $0.6\text{--}2.5M_\odot$, where M_\odot is the mass of the Sun, and maximum central densities around $\rho_c \approx 10^{16}\text{--}10^{14}$ g/cm³ respectively [9,10]. Those densities are close to that of NS central regions. The radii of those BECS ($\approx 15\text{--}25$ km) are slightly higher than those expected for NS, but it can be diminished by considering the presence of a strong magnetic field that interacts with the neutral neutron pair through its magnetic moment [11,12]. Thus, magnetized BECS models would be useful to approach the description of NS cores in the limiting situation in which the core can be thought of as mostly composed of paired neutrons [11].

In this paper, we aim to go deep into this possible connection between BECS and NS cores by taking into consideration the effects of a finite temperature on BECS models. We will consider a naked star fully composed of interacting bosons. The inclusion of other particles and a crust is needed to establish a more realistic connection between BECS and NS, but they are out of the scope of this article and will be tackled in future work. We would also like to remark that we are using the traditional name of “neutron star” to include not only canonical neutron star matter but also the other kind of

*gretica.qa@gmail.com

†lismarydelacaridad@gmail.com

‡On leave from Departamento de Física Teórica, Instituto de Cibernética Matemática y Física (ICIMAF), Cuba; aurorapm1961@usal.es

§hugo@icimaf.cu

exotic matter that could exist in the cores of NS [13]. Also, we are mainly interested in reproducing maximum masses around $2M_{\odot}$, although BECS models could also support observations of less massive ($\approx 0.77M_{\odot}$), smaller stars traditionally blamed on quark stars [12,14]. Besides, boson stars models have been largely exploited in the study of the hypothetical dark matter stars (see, for instance, [14–23]). In this context, the versatility of BECS comes to play since they allow to consider of several kinds of bosons (charged/neutral, scalar/vector, relativistic/Newtonian) (see, for instance, [14–23]) and situations (zero or finite temperature, magnetic field) starting from the same theoretical setup [10,11,14].

In previous studies of BECS under the action of a uniform and constant magnetic field [11,12] we found that, in general, these stars are spheroidal (because the magnetic field splits the pressure into two components, parallel and perpendicular to its axis), less massive, and smaller than the nonmagnetic ones. These effects begin to be noticeable for magnetic fields intensities $B \approx 10^{-2}B_c$ or higher, B_c being the boson critical field.¹ They are more relevant at low densities and depend on whether the magnetic field is constant or varies with the density.

Thermal effects have been traditionally ignored in the EoS of compact or exotic stars. In the case of fermion stars, the main argument behind the zero temperature approximation is that, given their high densities, the Fermi energy is much higher than any temperature achievable inside the star [24]. However, it was recently shown that even the canonical models of neutron stars allow temperatures that range from 10 to 100 MeV ($\approx 10^{11}$ – 10^{12} K) for densities around 10^{14} – 10^{15} g/cm³ [25–27]. The effects of these temperatures are not negligible: they change the internal composition and the macroscopic properties of those stars.

Boson systems are much more sensitive to environmental changes (variations in particle density, temperature, and magnetic field) due to the Bose-Einstein condensation [28–30]. In the case of BECS with nonrelativistic EoS, a finite temperature increases the pressure at low densities, increasing the size and mass of the stars [8,10]. When compared to the magnetized BECS described above, it appears, at first glance, that the thermal and magnetic effects oppose each other and that they should cancel out. But, as we shall see, this is not the case.

Hot BECS without magnetic field had been studied in previous works [8,10]. Our goal now is to study the joint role of temperature and magnetic field on their micro and macroscopic properties by considering the bosons as spin-1 relativistic particles. Spin-1 bosons are of interest due to their unique magnetic properties in connection with the condensate (see [11,28,30,31] for a discussion on the so-called Bose-Einstein ferromagnetism and its possible applications). They may arise as bound states of spin- $\frac{1}{2}$ fermions, as in the core of NS, but also as fundamental particles in the context of the standard model and its extensions [21,32]. The consideration of relativistic bosons is required to correctly account

for the effects of the super-strong magnetic fields that may be produced in astrophysical environments (up to 10^{18} G in the core of NS [33]). For such high intensities, the magnetic field energy might easily become comparable with the rest mass and the thermal energy of the particles and the magnetized vacuum contributes to the system with non-negligible energy, pressure, and magnetization [30,34].

The paper is organized as follows: We devote Sec. II to the EoS of magnetized BECS at finite temperatures. In Sec. III we present the structure equations that we use to obtain the macroscopic properties of these stars. Later in this section, we discuss the dependence on temperature of the properties of nonmagnetized BECS, with emphasis on the stars' stability and evolution, and finally we analyze the interplay of the thermal and magnetic effects. Concluding remarks are given in Sec. IV.

We use natural units $\hbar = c = 1$, and for numerical calculations we consider a spin-1 boson with mass $m = 2m_N$ and magnetic moment $\kappa = 2\mu_N$, m_N and μ_N being the mass and the magnetic moment of the neutron. In the plots, we use $a = 13$ fm. The choice of these values responds to our wish of maintaining the link between BECS and massive NS cores. However, the discussions of our results are valid for any hot BECS with a magnetic field, in particular also for dark matter BECS. Regarding the last ones, our calculations of several directly observable magnitudes, such as the mass and redshift, may contribute to the detection and classification of those exotic stars.

II. EQUATIONS OF STATE OF MAGNETIZED BOSE-EINSTEIN CONDENSATE STARS AT FINITE TEMPERATURE

The Hamiltonian of a gas of interacting bosons can be written as a sum of an ideal gas Hamiltonian \hat{H}_{th} that includes the effects of temperature and any external field, plus the particle-particle interaction Hamiltonian \hat{H}_{int} ,

$$\hat{H} = \hat{H}_{\text{int}} + \hat{H}_{\text{th}}. \quad (1)$$

Then, the grand thermodynamic potential per unit volume of the system is [10,11]

$$\Omega = \Omega_{\text{int}} + \Omega_{\text{th}}. \quad (2)$$

The boson-boson interaction is considered as a two-body contact interaction, i.e., we assume that only the low-energy binary collisions are relevant [9–11]. This approximation holds as far as the quantum fluctuations are negligible (mean field approximation), but this is expected for a dense system such as the BECS ($\rho \approx 10^{14}$ – 10^{15} g/cm³) at the relatively low temperatures needed for the existence of the condensate.

Despite its simplicity, the assumption of a two-body contact interaction allows one to obtain thermodynamic consistent EoS for a gas of interacting bosons at finite temperature [10] or magnetic field [11], whose corresponding mass-radius curves have maximum values and shapes that are consistent with other BECS models [8,9]. Hence, this is a useful starting point to understand the physics of hot magnetized BECS.

¹The critical field is defined as the field at which the magnetic energy of the particle equals its mass.

Under this assumption, Ω_{int} transforms into [10]

$$\Omega_{\text{int}} = 1/2u_0\rho_T^2, \quad (3)$$

where $u_0 = 4\pi a/m$ indicates the strength of the interaction and ρ_T is the density of particles and antiparticles, although as we shall see, the effects of antiparticles are negligible.

To compute Ω_{th} we start with its definition in the one-loop approximation (i.e., without radiative corrections) [30],

$$\begin{aligned} \Omega_{\text{th}}(\mu, T, B) &= \Omega_{\text{st}}(\mu, T, B) + \Omega_{\text{vac}}(B) \\ &= \sum_s \int_0^\infty \frac{p_\perp dp_\perp dp_3}{(2\pi)^2 \beta} \ln(f_{BE}^+ f_{BE}^-) \\ &\quad + \sum_s \int_0^\infty \frac{p_\perp dp_\perp dp_3}{(2\pi)^2} \varepsilon(p_3, p_\perp, B, s). \end{aligned} \quad (4)$$

Here μ is the chemical potential, $\beta = 1/T$ is the inverse of the temperature T , B is the magnetic field intensity, and $f_{BE}^\pm = [1 - e^{-(\varepsilon \mp \mu)\beta}]^{-1}$ are the distribution functions for particles/antiparticles. The sum over $s = 0, \pm 1$ runs over the spin states, p_3 and p_\perp are the momentum components parallel and perpendicular to the magnetic field axis, and ε is the energy spectrum of the vector bosons under an external magnetic field in the z direction [34],

$$\varepsilon(p_3, p_\perp, B, s) = \sqrt{m^2 + p_3^2 + p_\perp^2 - 2\kappa s B \sqrt{p_\perp^2 + m^2}}, \quad (5)$$

where

$$\varepsilon_{\text{gs}} = \varepsilon(p_3 = 0, p_\perp = 0, B, s = 1) = m\sqrt{1 - 2\kappa B/m} \quad (6)$$

is the ground state energy of the bosons. Note that the magnetic field couples with the transversal momentum of the particles, but contrary to what happens for charged bosons p_\perp is not quantized. That is because the appearance of Landau quantization is a consequence of the coupling among the magnetic field and the charge, but the bosons we are studying are neutral [34].

The first integral in Eq. (4), Ω_{st} , accounts for the statistical contribution of particles and antiparticles and depends on T , B , and μ . Using the Taylor expansion of the logarithm and integrating over the momentum components, Ω_{st} can be rewritten as [30]

$$\begin{aligned} \Omega_{\text{st}}(b, \mu, T) &= - \sum_s \sum_{n=1}^\infty \frac{e^{n\mu\beta} + e^{-n\mu\beta}}{2\pi^2 n\beta} \left\{ \frac{y_0^2}{n\beta^2} K_2(n\beta y_0) \right. \\ &\quad \left. - \alpha \int_{y_0}^\infty dx \frac{x^2}{\sqrt{x^2 + \alpha^2}} K_1(n\beta x) \right\}, \end{aligned} \quad (7)$$

where $K_l(x)$ is the McDonald function of order l , $y_0 = m\sqrt{1 - sb}$, $\alpha = smb/2$, and $b = \frac{B}{B_c}$ with $B_c = \frac{m}{2\kappa}$ the critical magnetic field of neutral vector bosons (for the numerical values of m and κ that we consider in the introduction for neutron stars cores $B_c = 7.8 \times 10^{19}$ G). Note that Eq. (7) holds for any temperature [30].

The second integral in Eq. (4) is the zero-point energy or vacuum term. It is independent of T and μ and has an

ultraviolet divergence. After renormalization it reads [30,34]

$$\begin{aligned} \Omega_{\text{vac}}(b) &= - \frac{m^4}{288\pi} [b^2(66 - 5b^2) - 3(6 - 2b - b^2)(1 - b)^2 \\ &\quad \times \ln(1 - b) - 3(6 + 2b - b^2)(1 + b)^2 \ln(1 + b)]. \end{aligned} \quad (8)$$

The thermodynamic potential of the interacting boson gas at finite temperature is obtained by adding Eqs. (3), (8), and (7) as $\Omega = \Omega_{\text{int}} + \Omega_{\text{st}} + \Omega_{\text{vac}}$. Thus, the EoS of the BECS can be computed as [10,11]

$$P_{\parallel} = -\Omega + \rho_T \left(\frac{\partial \Omega}{\partial \rho_T} \right)_{\mu, T, B}, \quad (9a)$$

$$P_{\perp} = -\Omega + \rho_T \left(\frac{\partial \Omega}{\partial \rho_T} \right)_{\mu, T, B} - MB, \quad (9b)$$

$$E = \Omega + \mu \left(\frac{\partial \Omega}{\partial \mu} \right)_{T, B} - T \left(\frac{\partial \Omega}{\partial T} \right)_{\mu, B}, \quad (9c)$$

$$\rho = \rho_{\text{gs}} - \left(\frac{\partial \Omega}{\partial \mu} \right)_{T, B}, \quad (9d)$$

$$\mathcal{M} = - \left(\frac{\partial \Omega}{\partial B} \right)_{T, \mu}, \quad (9e)$$

where P_{\parallel} and P_{\perp} are the pressures along and perpendicular to the magnetic axis, E is the internal energy, \mathcal{M} is the magnetization, and ρ is the particle density of the system. Note that ρ includes the condensed particles' ρ_{gs} as well as the difference of the particle/antiparticle densities in the excited states, $-\left(\frac{\partial \Omega}{\partial \mu}\right)_{T, \mu}$. Note that ρ differs from ρ_T in that the former contains the subtraction while the latter contains the sum of particle and antiparticle number density.

To complete the EoS of the magnetized compact object, the energy density and pressures of the magnetic field have to be taken into account since it also contributes to the hydrodynamic equilibrium and the gravitational mass of the star [35]. To do so in the case of a uniform and constant magnetic field, the so-called Maxwell contribution, $B^2/8\pi$, is added to E and P_{\perp} and subtracted from P_{\parallel} .

After derivation and simplification, the EoS of the hot magnetized BECS read

$$P_{\parallel} = \frac{1}{2}u_0\rho_T^2 - \Omega_{\text{st}} - \Omega_{\text{vac}} - \frac{B^2}{8\pi}, \quad (10a)$$

$$P_{\perp} = \frac{1}{2}u_0\rho_T^2 - \Omega_{\text{st}} - \Omega_{\text{vac}} - \mathcal{M}B + \frac{B^2}{8\pi}, \quad (10b)$$

$$E = \frac{1}{2}u_0\rho_T^2 + m\rho_{\text{gs}} + E_{\text{st}} + \Omega_{\text{vac}} + \frac{B^2}{8\pi} \quad (10c)$$

$$\rho = \rho_{\text{gs}} + \rho^+ - \rho^-, \quad (10d)$$

$$\mathcal{M} = \frac{\kappa}{\sqrt{1 - b}}\rho_{\text{gs}} + \mathcal{M}_{\text{st}} + \mathcal{M}_{\text{vac}}, \quad (10e)$$

with

$$E_{\text{st}} = -\Omega_{\text{st}} + \sum_s \sum_{n=1}^{\infty} \frac{e^{n\mu\beta} + e^{-n\mu\beta}}{n} \left\{ \frac{y_0^3 T}{4\pi^2} [K_1(n\beta y_0) + K_3(n\beta y_0)] + \frac{\alpha n}{2\pi^2} \int_{y_0}^{\infty} dx \frac{x^3}{\sqrt{x^2 + \alpha^2}} K_0(n\beta x) \right\}, \quad (11)$$

$$\rho^{\pm} = \sum_s \sum_{n=1}^{\infty} \frac{e^{\pm n\mu\beta}}{2\pi^2} \left\{ \frac{y_0^2}{n\beta} K_2(n\beta y_0) + \alpha \int_{y_0}^{\infty} dx \frac{x^2}{\sqrt{x^2 + \alpha^2}} K_1(n\beta x) \right\}, \quad (12)$$

and

$$\mathcal{M}_{\text{st}} = \sum_s \frac{\kappa s}{\pi^2 \beta} \sum_{n=1}^{\infty} \frac{e^{n\mu\beta} + e^{-n\mu\beta}}{n} \left\{ \frac{m y_0}{(2-b)s} K_1(n\beta y_0) + \int_{y_0}^{\infty} dx \frac{x^4}{2(x^2 + \alpha^2)^{3/2}} K_1(n\beta x) \right\}, \quad (13)$$

$$\mathcal{M}_{\text{vac}} = -\frac{\kappa m^3}{72\pi} \{7b(b^2 - 6) - 3(2b^3 - 9b + 7) \ln(1-b) - 3(2b^3 - 9b - 7) \ln(1+b)\}. \quad (14)$$

Here ρ^+ and ρ^- are the particle and antiparticle densities respectively.

To determine the range of temperatures to use in our study of BECS, let us focus first on the Bose-Einstein condensation of the magnetized gas. The condition for the condensation to occur is $\mu = m\sqrt{1-b}$ and $\rho_{\text{gs}} = 0$ [34]. Imposing this in Eq. (10d) we get the following expression for the implicit dependence of ρ , T , and B in the transition points (the critical curve) [30]:

$$\rho_c = \sum_s \sum_{n=1}^{\infty} \frac{e^{nm\sqrt{1-b}\beta} - e^{-nm\sqrt{1-b}\beta}}{2\pi^2} \left\{ \frac{y_0^2}{n\beta} K_2(n\beta y_0) + \alpha \int_{y_0}^{\infty} dx \frac{x^2}{\sqrt{x^2 + \alpha^2}} K_1(n\beta x) \right\}. \quad (15)$$

In Fig. 1 we show, for $B = 0$ and $B = 10^{17}$ G, the critical curves [Eq. (15)] in the ρ - t plane (where $t = T/m$). The gas is condensed in the shadowed regions. For fixed ρ , increasing the temperature destroys the condensation, while, for fixed t , increasing the density drives the system to the condensate. A finite magnetic field increases the shadowed region, thus favoring condensation. This enhancing effect of the magnetic field on the condensation is a consequence of the way it modifies the ground state of the gas [30]. As a general rule, the critical temperature of BEC depends on the inverse of the rest mass of the bosons ε_{gs} , so that decreasing ε_{gs} increases the critical temperature and favors condensation. For the gas we are studying, $\varepsilon_{\text{gs}} = m\sqrt{1-2\kappa B/m}$. Thus, as B increases, ε_{gs} decreases, favoring condensation.

To guarantee we have stars with a fraction of the bosons in the condensate, we need to restrict our study to the regions of the EoS where BEC exists. To do so, we will analyze

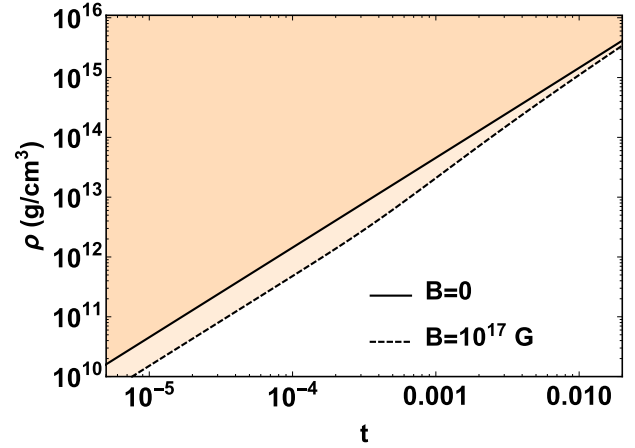


FIG. 1. The phase diagram of Bose-Einstein condensation in the density-temperature plane for $B = 0$ and $B = 10^{17}$ G. The BEC exists in the shadowed regions.

the dependence on T of the fraction of particles, antiparticles, and condensed particles (ρ^+/ρ_T , ρ^-/ρ_T and ρ_{gs}/ρ_T respectively) to select a range of temperatures that fulfill the previous requirement. In Fig. 2 we show those quantities as functions of ρ for several values of the temperature and $B = 0$. The vertical lines mark the critical density of condensation: for densities at their right, a fraction of the gas is in the condensed state. The region where the Bose-Einstein condensation exists decreases with the increase in temperature. Moreover, note that only for $T \leq 0.01m \approx 10^{11}$ K does the gas condense at densities around the typical central densities of BECS (10^{15} – 10^{16} g/cm³). In this regard, we will restrict our analysis of hot magnetized BECS to temperatures such that $T \leq 0.01m$, to guarantee the existence of Bose-Einstein condensation at least in some region inside the star.

For $T \leq 0.01m$, the antiparticle density is negligible (Fig. 2) and they will not have any relevant influence on the hot BECS physics. This situation does not change at a finite magnetic field, since to affect antiparticle production and Bose-Einstein condensation, B needs to be above $\approx 0.1B_c$, which for $B_c = 7.8 \times 10^{19}$ G is an order above the highest values of the magnetic field expected in compact stars [30]. Concerning the EoS Eq. (10), this means that $\rho_T = \rho$.

With the antiparticles out of the picture, at $B = 0$ the main effect of a finite temperature in the BECS EoS, Fig. 3(a), is an increase of the pressure for the lower energy densities ($E \leq 100$ MeV/fm³). This happens because, as T increases from 0, the thermal pressure $-\Omega_{\text{st}}(b, \mu, T)$ starts to gain relevance in comparison to the other components of the pressure. At high densities the boson-boson interaction pressure [$u_0 \rho_T^2/2$ in Eqs. (10a) and (10b)] prevails, being the total pressure corresponding to those densities barely affected by the temperature [Fig. 3(a)].

Turning on the magnetic field makes the pressure anisotropy noticeable [Fig. 3(b)]. In this case, as the density decreases, the parallel pressure Eq. (10a) (dashed lines) tends to $B^2/8\pi$ and becomes density independent, while the perpendicular pressure Eq. (10b) (solid lines) goes to $-B^2/8\pi$,

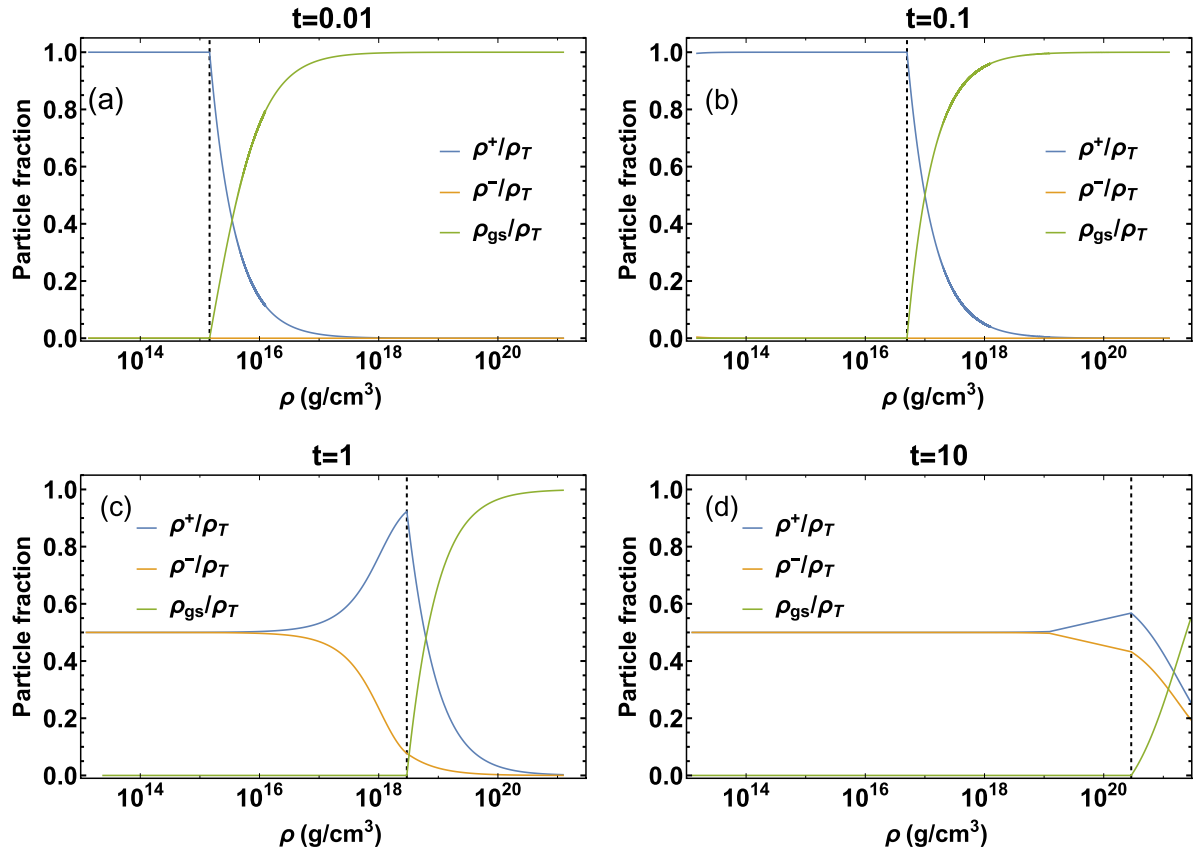


FIG. 2. Fraction of particles, antiparticles, and particles in the ground state as functions of ρ for several values of the temperature and $B = 0$. The vertical lines correspond to the density at which the condensate appears.

becoming negative. This instability imposes a lower bound on the densities that can exist inside the star for a given magnetic field [11]. The direct relation between the anisotropy in the pressures and the Maxwell pressure $\pm B^2/8\pi$ can be also appreciated by plotting the EoS of the magnetized star without those terms (Fig. 4) and checking that in that case the instability disappears.

The anisotropy in the pressure and the instability caused by the magnetic field persist for all the considered temperatures [Fig. 3(b)]. The magnetic energy per boson in units

of mass at $B = 10^{17}$ G, $\kappa B \approx 10^{-4}m$, is lower than the thermal energy $5 \times 10^{-4} - 10^{-2}m$, at all the temperatures used, except when $T = 0$. This may suggest that the increase in thermal pressure should be enough to balance the instability. However, what turns on the anisotropy is the term corresponding to the Maxwell classical energy of the magnetic field: $B^2/8\pi$. This term adds, or subtracts, to the pressures an energy per boson $B^2/8\pi\rho$ that is almost negligible at high densities, $B^2/8\pi\rho \approx 10^{-5}m$ for $E \approx 10^4$ MeV/fm³, but that leads the system behavior at the low ones: $B^2/8\pi\rho \approx 10^{-2}m$ for

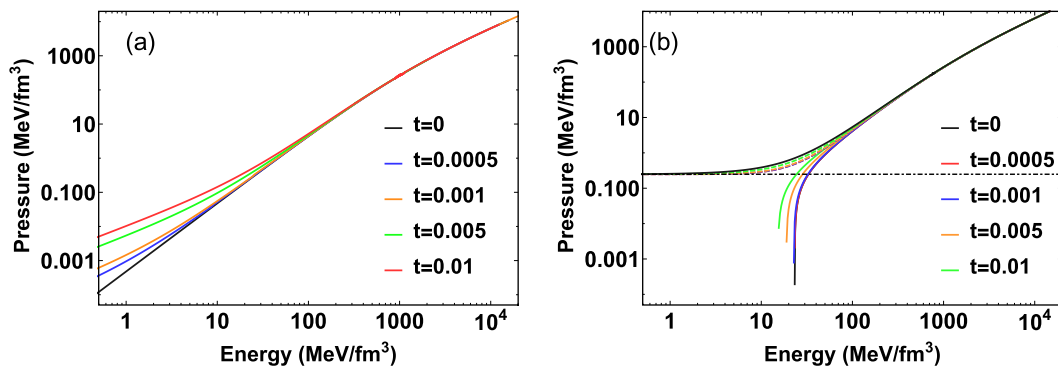


FIG. 3. The EoS of hot BECS with $B = 0$ (a) and $B = 10^{17}$ G (b). In (b), the dashed and solid lines correspond to the parallel and perpendicular pressures respectively, and the horizontal line signals the value of the Maxwell pressure $B^2/8\pi$ for $B = 10^{17}$ G.

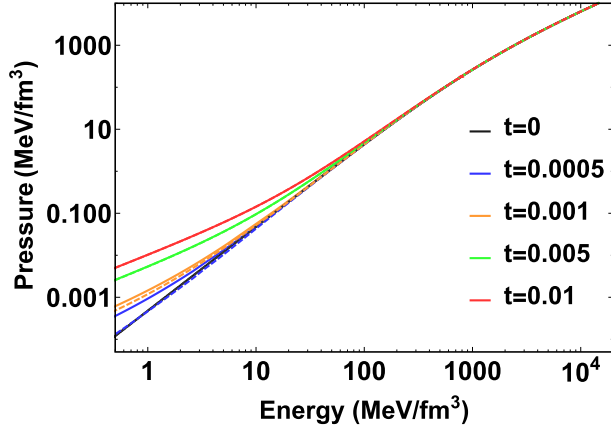


FIG. 4. The EoS of hot BECS with $B = 10^{17}$ G and no Maxwell contribution $\pm B^2/8\pi$ in the energy and pressures. The dashed and solid lines correspond to the parallel and perpendicular pressures respectively.

$E \approx 10 \text{ MeV/fm}^3$. Hence, the EoS in Fig. 3(b) is dominated by the magnetic field at low densities, by the temperature at the intermediate ones, and by the interactions at the highest values of E . So, the selected values of T and B guarantee that we will study stars where both their effects are relevant, although dependent on the density and on the assumption of constant magnetic field intensity.

III. MACROSCOPIC PROPERTIES OF RELATIVISTIC BOSE-EINSTEIN CONDENSATE STARS AT A FINITE TEMPERATURE UNDER THE ACTION OF A MAGNETIC FIELD

Now we focus on both thermal and magnetic effects on the macroscopic properties of BECS. To do so, we will assume that the temperature is constant inside the star. The temperature of compact stars is thought to increase toward the center [26,27]. However, detailed calculations of the inner profiles of NS with realistic EoS show that the increase of T is usually no greater than one order of magnitude and that the biggest change takes place near the surface of the star [26,36]. Thus considering a constant temperature is a good approximation. Similarly, self-consistent numerical calculations with realistic models for the inner magnetic fields of white dwarfs and neutron stars show that variations in the magnetic field intensity inside these objects do not usually exceed one order of magnitude [26,37,38]. Hence, we also assume that, inside the star, the magnetic field is uniform and constant, although at the end of Sec. III B we briefly discuss how the magnetic effects change when a field intensity dependent on the density is considered.

As discussed in the previous section, the magnetic field splits the inner pressure of the star into two components, one along and the other perpendicular to the magnetic axis. Since the inner pressure of compact objects is, in general, proportional to its radius [33], magnetized stars are not spherical but axially deformed. As a consequence, the macroscopic structure of a magnetized compact object cannot be accounted

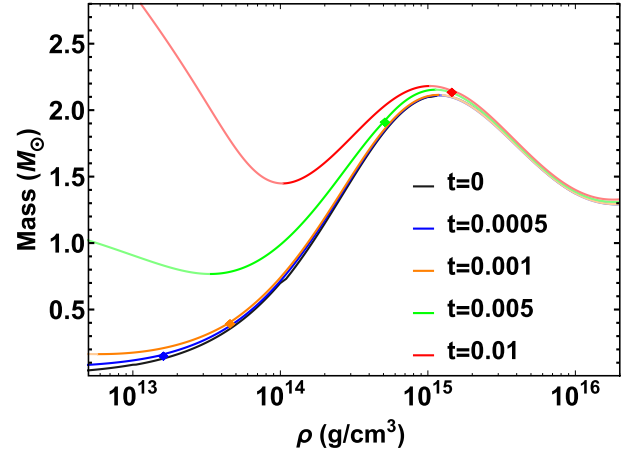


FIG. 5. The mass vs the central mass density of nonmagnetized BECS with different inner temperatures and $B = 0$.

for with the standard Tolman-Oppenheimer-Volkoff (TOV) equations [24] because they describe static spherically symmetric stars and do not admit a pressure anisotropy of the type caused by the magnetic field. To properly take into account the anisotropy, we will use the so-called γ -structure equations, given as [39]

$$\frac{dM}{dr} = \gamma r^2 \frac{(E_{\parallel} + E_{\perp})}{2}, \quad (16a)$$

$$\frac{dP_{\parallel}}{dr} = - \frac{(E_{\parallel} + P_{\parallel}) \left[\frac{r}{2} + 4\pi G r^3 P_{\parallel} - \frac{r}{2} \left(1 - \frac{2GM}{r}\right)^{\gamma} \right]}{r^2 \left(1 - \frac{2GM}{r}\right)^{\gamma}}, \quad (16b)$$

$$\frac{dP_{\perp}}{dr} = - \frac{(E_{\perp} + P_{\perp}) \left[\frac{r}{2} + 4\pi G r^3 P_{\perp} - \frac{r}{2} \left(1 - \frac{2GM}{r}\right)^{\gamma} \right]}{r^2 \left(1 - \frac{2GM}{r}\right)^{\gamma}}. \quad (16c)$$

These equations establish the hydrodynamic equilibrium between the gravity and the internal pressure of a spheroidal compact object, provided it is close to the spherical shape ($\gamma \approx 1$) [39]. In them, G is Newton's gravitational constant and $M(r)$ is the mass enclosed in the spheroid of equatorial radius r . To obtain the total mass and radius of the star, Eqs. (16) are integrated with the initial conditions $E_0 = E(r=0)$, $P_{\parallel 0} = P_{\parallel}(r=0)$, and $P_{\perp 0} = P_{\perp}(r=0)$, where E_0 , and $P_{\perp 0}$ and $P_{\parallel 0}$ are taken from the EoS, while the condition $P(R) = 0$ defines the star equatorial radius from which the total mass $M(R)$ is computed. At each integration step, E_{\parallel} and E_{\perp} are computed using the parametric dependence of the energy in each pressure derived from Eqs. (10a) and (10b).

The parameter γ accounts for the axial deformation of the star and relates the polar and equatorial radii as $z = \gamma r$ ($Z = \gamma R$) such that if $\gamma = 1$ the star is spherical while for $\gamma > 1$ ($\gamma < 1$) it is a prolate (oblate) spheroid. In Eq. (16) γ acts as an external parameter [39]. To solve them, in [39] γ has been considered as the ratio between the parallel and the perpendicular central pressures,

$$\gamma = P_{\parallel 0}/P_{\perp 0}. \quad (17)$$

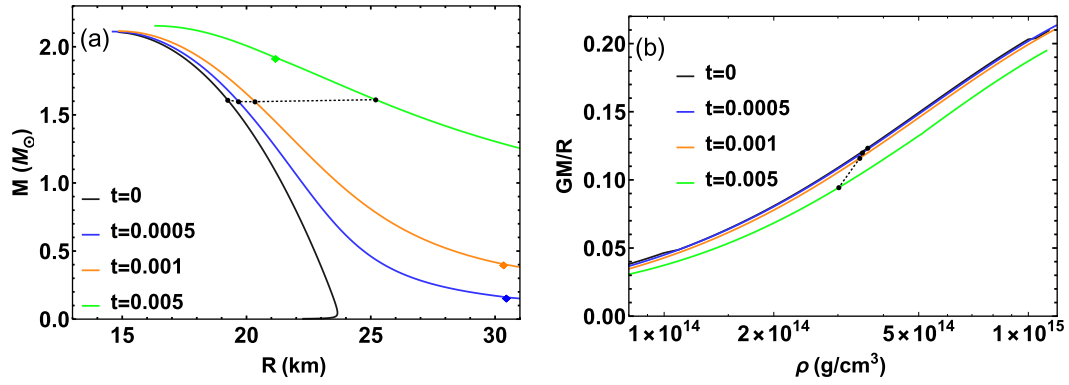


FIG. 6. Mass-radius diagram (a) and compactness (b) of BECS at different temperatures and $B = 0$; in this case, since $B = 0$ the star is spherical and the polar and equatorial radii coincide ($Z = R$). The black dots mark the position on each of the curves of a star with baryon mass of $1.7M_{\odot}$ (composed of around 10^{57} bosons); they have been joined with a dotted line for a better visualization of the star evolution as the temperature decreases (see the text).

This ansatz connects the system's geometry with its physical properties and follows from the proportionality between the radius and the central pressure of spherical stars [33]. When $B = 0$, $P_{\perp} = P_{\parallel}$, $\gamma = 1$, Eq. (16) reduced to TOV equations and the spherical case is recovered. For $B \neq 0$, the axial symmetry of Eq. (16) is compatible with a dipolar magnetic field in the star. Regardless of their approximated characteristics, the study of the macroscopic structure of magnetized compact objects through the combination of Eq. (16) with the ansatz Eq. (17) yields reasonable results [11,12,39–41], that are qualitatively similar to those coming from models that consider more sophisticated magnetic field geometries [26,36–38,42,43].

Equation (16) guarantee the hydrodynamic equilibrium for spheroidal stars, but equilibrium does not necessarily imply stability [2,24,41,44]. We use two criteria to study the stability of the solutions. The first one guarantees stability against radial oscillations and requires that $dM/d\rho \geq 0$ [24]. The second criterion requires $M(\rho) < M_B(\rho)$, where M_B is the baryonic mass of the star, Eq. (18), and assures stability

against the dispersion of the particles forming the star [2,24]:

$$M_B = m \int_0^R \frac{4\pi r^2 \rho(P(r))}{\left(1 - \frac{2GM(r)}{r}\right)^{\gamma/2}} dr. \quad (18)$$

Since the solution of Eqs. (16) gives two radii, to compare with the $B = 0$ case it is convenient to use the mean radius R_m so that the surface of the sphere it determines is equal to the surface of the spheroidal star,

$$A = 2\pi R \left(R + \frac{Z}{\epsilon} \arcsin \epsilon \right), \quad (19)$$

where $\epsilon = \sqrt{1 - \gamma}$ is the ellipticity [41].

Apart from the mass and radii, we are also interested in analyzing the thermal and magnetic effects over the compactness GM/R , the gravitational redshift [41]

$$z = \frac{1}{\left(1 - \frac{2GM}{R}\right)^{\gamma/2}} - 1, \quad (20)$$

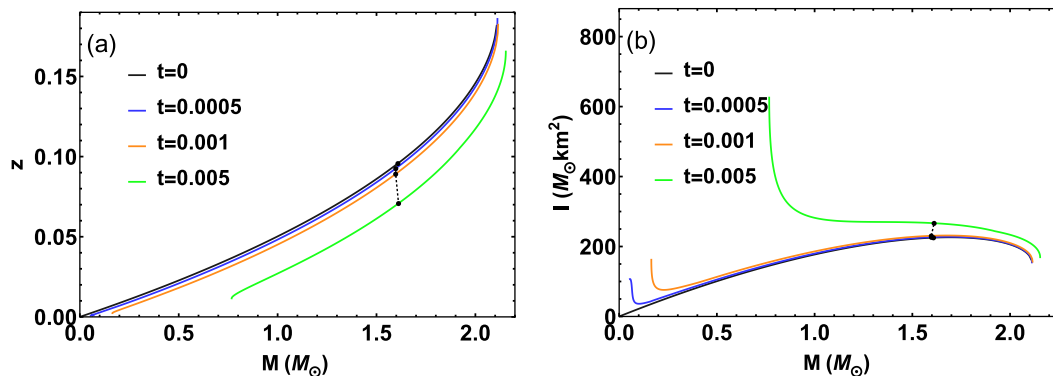


FIG. 7. Gravitational redshift (a) and moment of inertia as functions of the mass of the star (b) for several values of the temperature and $B = 0$. The black dots mark the position on each curve of the star with baryon mass of $1.7M_{\odot}$; they have been joined with a dotted line for a better visualization of the star evolution as the temperature decreases.

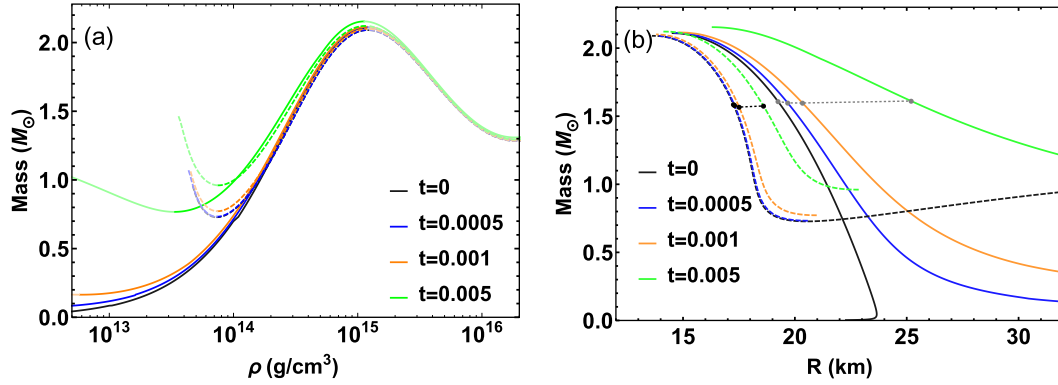


FIG. 8. Mass–central-density (a) and mass–mean radius R_m (b) curves for BECS at several temperatures and magnetic field $B = 10^{17}$ G (dashed curves) and $B = 0$ (solid curves). The black dots in (b) mark the position on each curve of the star with baryon mass of $1.7M_{\odot}$; they have been joined with a dotted line for a better visualization of the star evolution as the temperature decreases.

and the mass quadrupolar moment [41]

$$Q = \frac{\gamma}{3}(M/M_{\odot})^3(1 - \gamma^2); \quad (21)$$

this last equation is only for magnetized stars, since for spherical stars $Q = 0$. In the case of nonmagnetized stars at a finite temperature, we show the moment of inertia I instead of Q :

$$I = \int_0^R 4\pi r^4 E(P(r)) dr. \quad (22)$$

A. Nonmagnetized Bose-Einstein condensate stars at finite temperature

We will first concentrate on understanding the effects of temperature on nonmagnetized relativistic BECS. Figure 5 shows the masses of the stars that result from solving the γ -structure equations with the EoS at $B = 0$ [Fig. 3(a)]. The increase that the temperature causes in the pressure at low densities provokes an increase in the masses of the stars compared to the zero temperature case. This behavior has been observed for nonrelativistic BECS and white dwarfs in [10] and [38] respectively. What we found unexpected is that the temperature affects the stability of BECS.

In Fig. 5 the unstable sections of the curves have a lighter color. The stability analysis reduced to looking for the region where $\partial M/\partial \rho \geq 0$, since the baryonic mass criterion is always fulfilled for a broader range of central densities. The interval of central densities of stable stars gets smaller as the temperature increases. Table I collects the extreme values of the central mass density and the mass of the stable stellar configurations for each temperature. The variation with T of the maximum mass and its corresponding central density is almost negligible, while the minimum mass and central density remarkably increase with the temperature. Hence, one expects that, even if we allow $T > 0.01m$, there would be a temperature beyond which there are no stable stars in the range of central densities considered. At such high temperatures, the statistical pressure $-\Omega_{\text{st}}$ becomes so high that a gravitationally bound structure cannot form. In the remaining figures of this section, we show only the stable part of the curves.

The squares over the curves in Fig. 5 signal the value of the central density beyond which there are no condensed bosons inside the star. As shown in this plot, the condensation disappears from the interior of the stable stars as the temperature increases (the squares move to the right). For $t = 0.01$ any star in the stable region contains Bose-Einstein condensation, although the qualitative behavior of the mass–central-density curve does not change. This may be a consequence of the fact that, ultimately, what sustains the star is the pressure due to the interaction of the bosons. Anyhow, we will restrict our following discussions to those temperatures where the condensation is present at least in some part of the stable stellar sequence.

Apart from increasing the mass and reducing the number of stable stars, the temperature increases the radius of the stars [Fig. 6(a)]. As a consequence, the compactness of hot BECS decreases with T , indicating that the hotter stars are less denser [Fig. 6(b)]. An interesting feature of having BECS at different temperatures is that, for a fixed baryon mass, one can compare how the macroscopic properties of the star evolve as it gets colder and older. We made this for a star with a baryon mass of $1.7M_{\odot}$ (composed by around 10^{57} bosons). The position of this star is marked with black dots on Figs. 6 and 7. Especially from Fig. 6(b), we can see how the star becomes denser as its temperature decreases. This is caused by the reduction in the radius since the gravitational mass

TABLE I. Extreme values of the central mass density and the total mass of the stable stellar configurations at finite temperature and zero magnetic field.

	ρ_{\min} (10^{11} g/cm 3)	ρ_{\max} (10^{15} g/cm 3)	M_{\min} (M_{\odot})	M_{\max} (M_{\odot})
$t = 0$		1.23		2.11
$t = 0.0005$	3.10	1.19	0.05	2.11
$t = 0.001$	9.72	1.18	0.16	2.11
$t = 0.005$	336	1.12	0.77	2.15
$t = 0.01$	1034	1.03	1.45	2.18

TABLE II. Extreme values of the central mass density and the total mass of the stable stellar configurations at finite temperature and magnetic field.

	ρ_{\min} (10^{13} g/cm ³)		ρ_{\max} (10^{15} g/cm ³)		M_{\min} (M_{sol})		M_{\max} (M_{sol})	
	$B = 0$	$B = 10^{17}$ G	$B = 0$	$B = 10^{17}$ G	$B = 0$	$B = 10^{17}$ G	$B = 0$	$B = 10^{17}$ G
$t = 0$		7.37	1.23	1.23		0.72	2.11	2.09
$t = 0.0005$	0.032	7.41	1.19	1.18	0.05	0.73	2.11	2.09
$t = 0.001$	0.580	7.49	1.18	1.18	0.16	0.77	2.11	2.10
$t = 0.005$	3.36	7.55	1.12	1.18	0.77	0.96	2.15	2.12

remains almost constant [Fig. 6(a)], indicating that the star contracts as it cools (its pressure decreases with T).

Finally, in Fig. 7 we show the change in temperature of the redshift (a) and the moment of inertia (b). The redshift increases with decreasing temperature, because the more compact a star is, the more relativistic it gets. As we can expect, following the same reasoning, the moment of inertia increases with temperature, since it is proportional to the radius of the star.

B. Magnetized Bose-Einstein condensate stars at finite temperature

In this section, we will analyze the interplay of temperature and magnetic field on the macroscopic properties of BEC, solving Eq. (16) with the EoS (10) at $B = 10^{17}$ G [Fig. 3(b)]. For a fixed temperature, a constant magnetic field reduces the number of star configurations at low densities [Fig. 8(a)]. Magnetized BECS has a lower bound in their central density at the point where P_{\parallel} becomes zero, and for that reason the mass–central-density curves are shorter when $B \neq 0$. In addition to this bound, the mass-central density curves of magnetized BECS have a minimum in the low-density region that reduces, even more, the number of stable stars (those that have $dM/d\rho > 0$). As a consequence, a lower bound appears for the total mass of magnetized BECS. This minimum mass of stable magnetized stars increases with t , while the maximum mass is barely affected by the temperature and the magnetic field (Table II). The range of allowed central densities in the stable stars goes from 10^{13} to 10^{15} g/cm³, which is compatible with the values of densities in the cores of neutron stars.

The magnetic field drastically reduces the size of the stars in both the polar and the equatorial directions. This can be appreciated from Fig. 8(b) through the reduction of the mean radius of the magnetized stars, but also from Fig. 9, where we draw the transversal section of the stars with the maximum mass in the polar-equatorial radius (Z - R) plane for each value of t and B . However, from Figs. 8(b) and 9 we can also appreciate that, for a high enough temperature, a hot magnetized BECS can attain masses and radii above those corresponding to the $B = 0$, $T = 0$ case (see the green curves corresponding to $t = 0.005$).

In Fig. 8(b) we consider the effect of the magnetic field on the evolution of a star of baryon mass of $1.7M_{\odot}$ (black dots on the plots). Similarly to $B = 0$, at $B = 10^{17}$ G the star becomes denser as its temperature decreases since its gravitational mass

remains almost constant while its radii diminish [Fig. 8(a)]. The only difference is that the gravitational mass of the hot magnetized star is slightly less than the one of the $B = 0$ case (gray dots on the plots). If we were to study the joint evolution of the temperature and the magnetic field as the star ages, we should consider a situation in which both magnitudes diminish. But it will be hard to anticipate whether the BECS will contract or expand since this will depend on the relative values of T and B .

Due to the reduction of the equatorial radius of magnetized stars, the compactness (GM/R) of magnetized hot BECS is above that of the $B = 0$, $T = 0$ case for all the considered temperatures [Fig. 10(a)]. The redshift also increases at a finite magnetic field, meaning that the star becomes more relativistic [Fig. 10(b)]. However, for a fixed magnetic field, the compactness increases with temperature for low density, while at higher densities decreases with T . Also from Fig. 10(b), we see that, as the star cools, its central density grows.

To explore the effects of the temperature on the deformation of the magnetized BECS, in Fig. 11(a) we show the equatorial (solid) and polar (dashed) radius R and Z as functions of the stars' central density for several values of the temperature. At $T = 0$, $B \neq 0$, $Z < R$, hence, the stars are oblate objects, and the difference between R and Z is higher at low densities, while it is negligible at the higher ones (that is why the transversal section of the stars in Fig. 9 is a circle). An increase in temperature increases R and Z without eliminating their difference. Thus, hot magnetized stars are still oblate and exhibit a nonzero mass quadrupolar moment that increases with T [Fig. 11(b)]. This happens because the hotter stars are more deformed than the colder ones [their γ is farther from one, Fig. 11(c)]. Note that Q depends directly on M and γ [Eq. (21)]. The values of Q for the more massive stars are close to zero since for those stars $\gamma \approx 1$. As the gravitational mass decreases, the behavior of Q changes according to temperature. For the smallest values of T , at which the magnetic effects dominate, Q attains a maximum value for an intermediate mass. This also happens for magnetized strange stars [41], and it is connected with the fact that at high mass γ goes to 1 ($P_{\parallel 0} \approx P_{\perp 0}$), and at lower mass γ decreases ($P_{\parallel 0} \rightarrow 0$). As T increases, the sequence of stable stars is reduced, the maximum disappears, and the lighter stars become the ones with the highest value of Q . Regarding gravitational waves, the behavior of Q with T implies that the temperature may enhance their emission for the stars of small and intermediate masses.

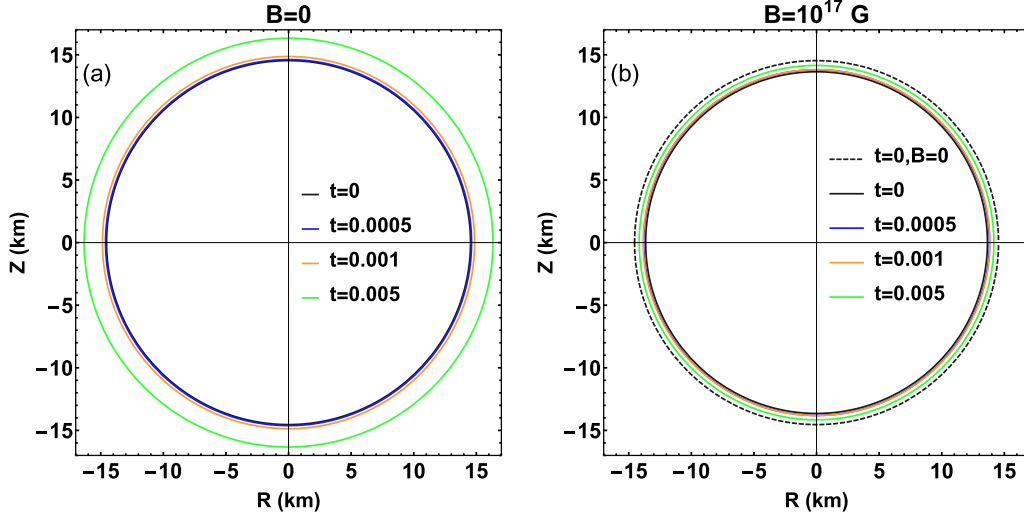


FIG. 9. The transversal section of the stars with the maximum mass in the polar-equatorial radii (Z - R) plane for several values of t and B . Due to their high inner densities, for these stars the magnetic deformation is negligible. The external circle in the plots is not a star but the angular scale.

Finally, we would like to point out that the thermal and magnetic effects we discussed may be subjected to variations in the way the temperature and magnetic field are modeled inside the stars. As an example, Figs. 12(a), 12(b), and 12(c) show the EoS and the mass-radius and mass-central-density curves of BECS with $t = 0.001$ and $B = 0$, $B = 10^{17}$ G and a density-dependent magnetic field $B(\rho) = B_{\text{cent}} + B_s(1 - e^{-\beta(\frac{\rho}{\rho_c})^\alpha})$ [45]. Here B_{cent} and ρ_c are the magnetic field and the density at the center of the star, $B_s = 10^{14}$ G is the surface magnetic field, and $\alpha = 3$ and $\beta = 0.05$ [Fig. 12(d)]. The central and surface values of B have been selected in the range of those corresponding to NS, although we remind the reader that the connection of BECS with NS is not straightforward. Note that, for all the temperatures here considered, the major decrease in the magnetic field is produced near the star's surface [Fig. 12(d)]. For $B = B(\rho)$ the anisotropy in the pressures becomes negligible, the low-density instability disappears [Fig. 12(a)], and the radii of the stars are larger than those corresponding to $B = 0$ [Fig. 12(a)]. However, in

this case, there still exists a lower bound for the central density of stable stars, and their masses are lower than those of non-magnetized stars with the same central density [Fig. 12(c)]. Our analysis of BECS with a density-dependent magnetic field also indicates that the use of a realistic temperature profile may attenuate but not erase the thermal effects we have discussed.

IV. CONCLUDING REMARKS

We obtained the EoS and the macroscopic properties of relativistic BECS at finite temperatures with a magnetic field. Such stars consist of a condensed gas of interacting neutral vector bosons coupled to a uniform and constant magnetic field. We assumed for the bosons a two-body contact interaction independent of the temperature and the magnetic field, while for the thermal part of the EoS we used the one-loop thermodynamic potential of a gas of free vector bosons at a finite temperature under the action of an

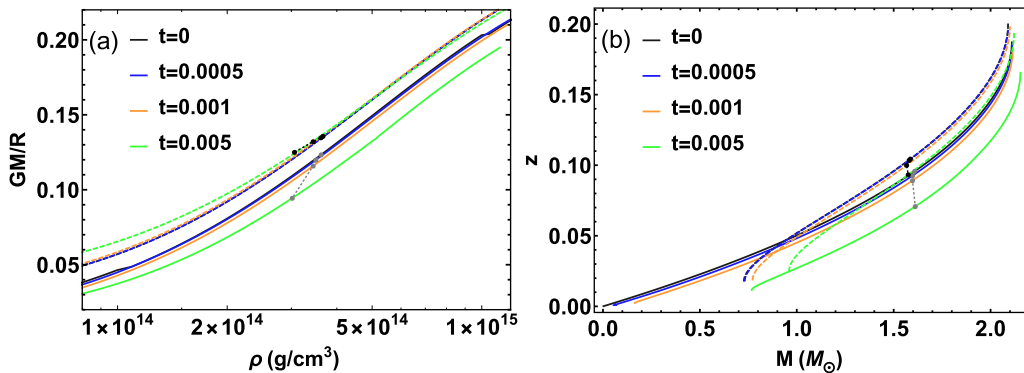


FIG. 10. Compactness (a) and gravitational redshift (b) for BECS at several temperatures and magnetic field $B = 10^{17}$ G (dashed curves) and $B = 0$ (solid curves). The black and gray dots mark the position on each curve of the star with baryon mass of $1.7M_{\odot}$; they have been joined with dotted lines for a better visualization of the star evolution as the temperature decreases.

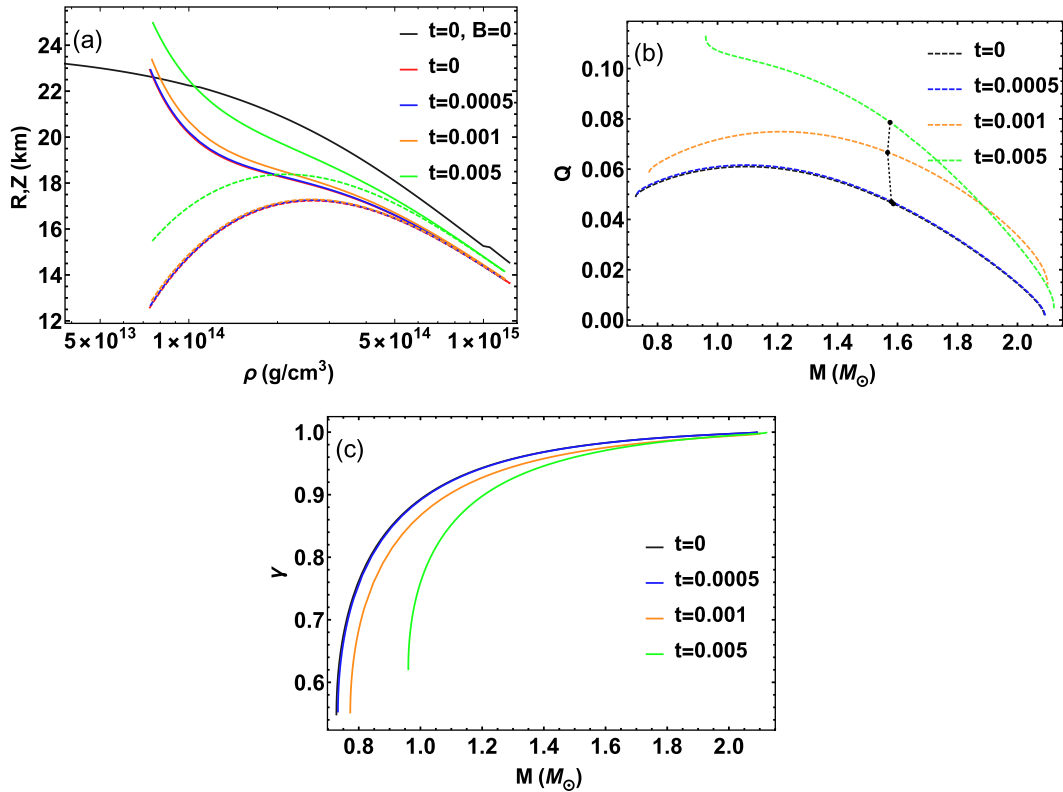


FIG. 11. Equatorial (solid) and polar (dashed) radii as a function of the central density for $B = 10^{17}$ G and several values of temperature (a). The mass quadrupolar moment as a function of the star mass (b). The parameter γ as a function of the star mass (c). In (a) the $B = 0$, $T = 0$ is included for reference. The black dots in (b) mark the position on each curve of the star with baryon mass of $1.7M_\odot$; they have been joined with a dotted line for a better visualization of the star evolution as the temperature decreases.

external magnetic field. To obtain the macroscopic properties we used the γ -structure equations; they mimic a dipolar magnetic field and can properly account for the anisotropy in the pressures.

Our study was restricted to temperatures two orders below the boson mass m . At $T > 0.01m$, the Bose-Einstein condensation is achieved at densities far beyond the central densities of stable stars. Thus, going above this limit does not preserve the nature of BECS. Since the antiparticles' density starts to be non-negligible at $T \geq m$, pair production has no relevance in our model. Finally, the values of T and B used in the plots were selected such that the thermal and magnetic energy is about the same order. This makes it possible to analyze the joint effects of T and B in the physics of the star.

At zero magnetic field, the main effect of the temperature in the EoS of BECS is to increase the pressure at low densities. It reflects later as an increase in the masses and radius of the stars. Thus hot BECS are bigger and heavier than their zero-temperature counterparts. These effects are more relevant for the stars with lower central densities and higher temperatures, while the maximum mass of the model is almost unchanged and remains mainly dominated by the microscopic properties of the bosons. The other relevant and unexpected feature related to the pure thermal effects is the existence of a lower bound on the central density of stable

stars. This lower allowable density increases with T , such that the higher the temperature, the fewer the number of stable BECS.

A constant magnetic field reduces, even more, the number of stable stars and provokes the BECS to axially deform in a manner that affects their size in all directions and other macroscopic properties. In general, magnetized BECS at finite T are smaller, denser, and more compact than nonmagnetized hot stars. Although increasing T increases the mass and the polar and equatorial radii of the magnetized stars, a finite temperature is not enough to erase either the anisotropy in the pressure or the instability caused by the magnetic field at low densities. Moreover, increasing the temperature favors the deformation and increases the value of the quadrupolar moment of the stars of small and intermediate masses, apparently enhancing gravitational waves' emission. Therefore, if at first sight it might seem that a finite temperature will cancel the magnetic field effects in BECS, it is clear from the results of our study that the interaction of T and B adds new and nontrivial features to the physics of these stars. As we also showed, a magnetic field dependent on the baryon density of the star erases the anisotropy, but still causes a reduction in the mass and number of stable stars, indicating that a more realistic model for the magnetic field and the temperature may attenuate but not eliminate their effects.

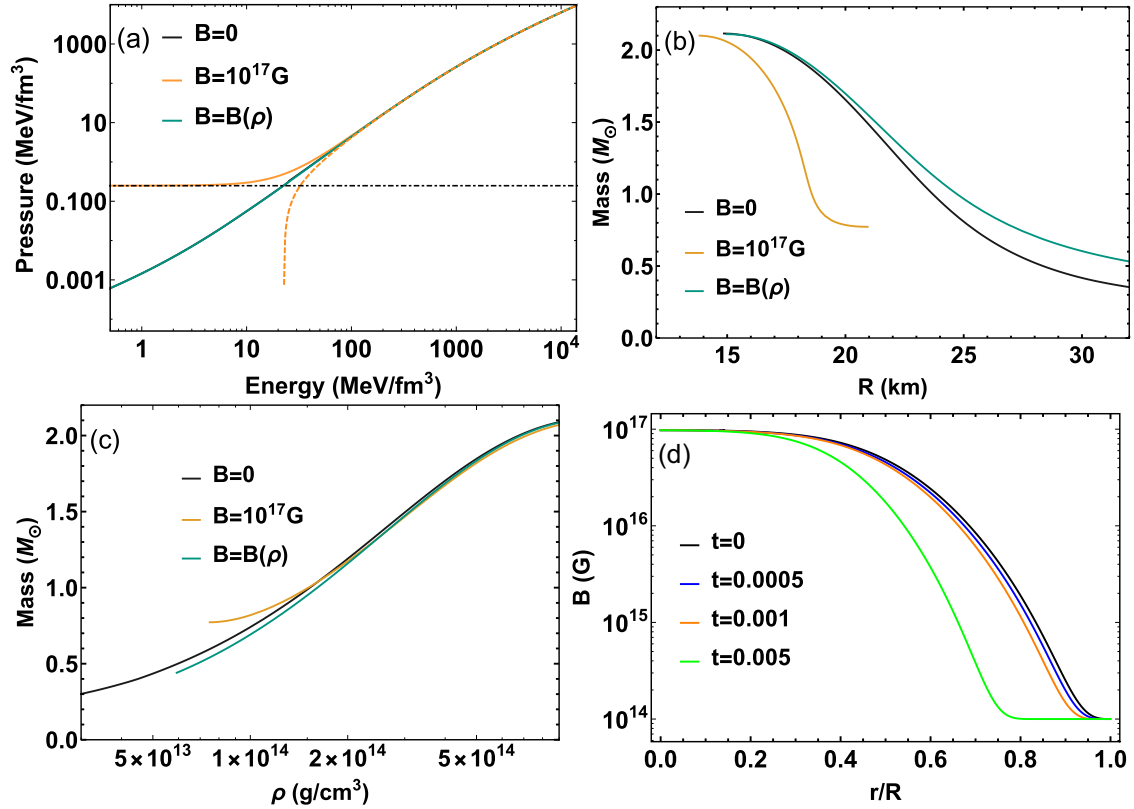


FIG. 12. BECS with $t = 0.001$ and $B = 0$, $B = 10^{17}$ G and inner magnetic field intensity dependent on the star particle density $B(\rho)$: EoS, the solid curves, correspond to the parallel pressure while the dashed ones correspond to the perpendicular pressure (a); mass-radius curves (b); mass–central-density curves (c). Inner magnetic field of the star versus its internal equatorial radius r (in units of the equatorial radius of the star R) for stars with $B(\rho)$, central density $\rho = 10^{15}$ g/cm³, and several temperatures (d).

Magnetized BECS models may be used as alternative models for the cores of NS. Indeed, the results indicate that hot magnetized BECS can account for the masses and inner densities of these cores, their radii being larger than the observed ones. However, the increase of B , as well as the decrease of T , may contribute to a readjustment of the radius without provoking considerable changes in the maximum mass of the stars. This indicates that a better coincidence with the observed properties of NS may be attained by fine tuning the parameter space of the model, combined with the

inclusion of some other features as a crust and other components of the star. We plan to explore those possibilities in future works.

ACKNOWLEDGMENTS

The work of G.Q.A, L.C.S.G, and H.P.R. was supported by Project No. NA211LH500-002 of AENTA-CITMA, Cuba. A.P.M. acknowledge the support of the Agencia Estatal de Investigación through the Grant PID2019-107778GB-I00 and from Junta de Castilla y León, SA096P20 project.

[1] R. Ruffini and S. Bonazzola, *Phys. Rev.* **187**, 1767 (1969).
 [2] M. Gleiser, *Phys. Rev. D* **38**, 2376 (1988).
 [3] E. Takasugi and M. Yoshimura, *Z. Phys. C* **26**, 241 (1984).
 [4] M. H. Anderson, J. R. Ensher, M. R. Matthews, C. E. Wieman, and E. A. Cornell, *Science* **269**, 198 (1995).
 [5] P. S. Shternin, D. G. Yakovlev, C. O. Heinke, W. C. G. Ho, and D. J. Patnaude, *Mon. Not. R. Astron. Soc. Lett.* **412**, L108 (2011).
 [6] D. Page, M. Prakash, J. M. Lattimer, and A. W. Steiner, Superfluid neutrons in the core of the neutron star in Cassiopeia A, [arXiv:1110.5116](https://arxiv.org/abs/1110.5116).

[7] D. Page, in *Electromagnetic Radiation from Pulsars and Magnetars*, Astronomical Society of the Pacific Conference Series Vol. 466, edited by W. Lewandowski, O. Maron, and J. Kijak (Astronomical Society of the Pacific, San Francisco, 2012), p. 161.
 [8] C. Gruber and A. Pelster, *Eur. Phys. J. D* **68**, 341 (2014).
 [9] P.-H. Chavanis and T. Harko, *Phys. Rev. D* **86**, 064011 (2012).
 [10] S. Latifah, A. Sulaksono, and T. Mart, *Phys. Rev. D* **90**, 127501 (2014).
 [11] G. Quintero Angulo, A. Pérez Martínez, H. Pérez Rojas, and D. Manreza Paret, *Int. J. Mod. Phys. D* **28**, 1950135 (2019).

- [12] G. Quintero Angulo, A. Pérez Martínez, and H. Pérez Rojas, *Astron. Nachr.* **340**, 909 (2019).
- [13] A. Schmitt, *Dense Matter in Compact Stars: A Pedagogical Introduction*, Lecture Notes in Physics Vol. 811 (Springer, Berlin, 2010).
- [14] X. Y. Li, T. Harko, and K. S. Cheng, *J. Cosmol. Astropart. Phys.* **2012**, 001 (2012).
- [15] E. Braaten and H. Zhang, *Rev. Mod. Phys.* **91**, 041002 (2019).
- [16] T. Rindler-Daller and P. R. Shapiro, *Mon. Not. R. Astron. Soc.* **422**, 135 (2012).
- [17] S. Davidson and T. Schwetz, *Phys. Rev. D* **93**, 123509 (2016).
- [18] X. Zhang, M. H. Chan, T. Harko, S.-D. Liang, and C. S. Leung, *Eur. Phys. J. C* **78**, 346 (2018).
- [19] J. F. Delgado, C. A. Herdeiro, and E. Radu, *J. Cosmol. Astropart. Phys.* **2020**, 037 (2020).
- [20] J. Ellis, G. Hütsi, K. Kannike, L. Marzola, M. Raidal, and V. Vaskonen, *Phys. Rev. D* **97**, 123007 (2018).
- [21] A. Belyaev, G. Cacciapaglia, J. McKay, D. Marin, and A. R. Zerwekh, *Phys. Rev. D* **99**, 115003 (2019).
- [22] D. Rafiei Karkevandi, S. Shakeri, V. Sagun, and O. Ivanytskyi, *Phys. Rev. D* **105**, 023001 (2022).
- [23] D. R. Karkevandi, S. Shakeri, V. Sagun, and O. Ivanytskyi, Tidal deformability as a probe of dark matter in neutron stars, *The Sixteenth Marcel Grossmann Meeting*, 3713 (2023), doi: 10.1142/9789811269776_0307.
- [24] M. Camenzind, *Compact Objects in Astrophysics: White Dwarfs, Neutron Stars and Black Holes*, Astronomy and Astrophysics Library (Springer, Berlin, 2007).
- [25] V. Dexheimer, D. P. Menezes, and M. Strickland, *J. Phys. G: Nucl. Part. Phys.* **41**, 015203 (2014).
- [26] B. Franzon, V. Dexheimer, and S. Schramm, *Phys. Rev. D* **94**, 044018 (2016).
- [27] J.-B. Wei, G. F. Burgio, A. R. Raduta, and H.-J. Schulze, *Phys. Rev. C* **104**, 065806 (2021).
- [28] L. Suárez-González, G. Quintero Angulo, A. Pérez Martínez, and H. Pérez Rojas, *J. Phys.: Conf. Ser.* **1239**, 012004 (2019).
- [29] L. de la Caridad Suárez González, G. Q. Angulo, A. P. Martínez, and H. P. Rojas, *Astron. Nachr.* **340**, 952 (2019).
- [30] G. Quintero Angulo, L. C. Suárez González, A. Pérez Martínez, and H. Pérez Rojas, *Phys. Rev. C* **104**, 035803 (2021).
- [31] K. Yamada, *Prog. Theor. Phys.* **67**, 443 (1982).
- [32] E. D. Nobile, [arXiv:1709.08700](https://arxiv.org/abs/1709.08700).
- [33] J. M. Lattimer and M. Prakash, *Astrophys. J.* **550**, 426 (2001).
- [34] G. Q. Angulo, A. P. Martínez, and H. P. Rojas, *Phys. Rev. C* **96**, 045810 (2017).
- [35] E. J. Ferrer, V. de la Incera, J. P. Keith, I. Portillo, and P. L. Springsteen, *Phys. Rev. C* **82**, 065802 (2010).
- [36] V. Dexheimer, B. Franzon, and S. Schramm, *J. Phys.: Conf. Ser.* **861**, 012012 (2017).
- [37] D. Chatterjee, J. Novak, and M. Oertel, *Phys. Rev. C* **99**, 055811 (2019).
- [38] J. Peterson, V. Dexheimer, R. Negreiros, and B. G. Castanheira, *Astrophys. J.* **921**, 1 (2021).
- [39] D. A. Terrero, V. H. Mederos, S. L. Pérez, D. M. Paret, A. P. Martínez, and G. Q. Angulo, *Phys. Rev. D* **99**, 023011 (2019).
- [40] S. L. Pérez, D. Manreza-Paret, G. Q. Angulo, A. Pérez Martínez, and D. Alvear Terrero, *Astron. Nachr.* **342**, 326 (2021).
- [41] D. A. Terrero, S. L. Pérez, D. M. Paret, A. P. Martínez, and G. Q. Angulo, *Phys. Rev. C* **103**, 045807 (2021).
- [42] R. Rizaldy and A. Sulaksono, *J. Phys.: Conf. Ser.* **1080**, 012031 (2018).
- [43] D. Chatterjee, T. Elghozi, J. Novak, and M. Oertel, *Mon. Not. R. Astron. Soc.* **447**, 3785 (2015).
- [44] S. L. Shapiro and S. A. Teukolsky, *Black Holes, White Dwarfs, and Neutron Stars: The Physics of Compact Objects* (John Wiley & Sons, New York, 2008).
- [45] D. Bandyopadhyay, S. Chakrabarty, and S. Pal, *Phys. Rev. Lett.* **79**, 2176 (1997).